doi:10.1093/plphys/kiab426 PLANT PHYSIOLOGY 2021: 187: 2393–2404

Plant Physiology®

Research Report

Dynamic changes in primexine during the tetrad stage of pollen development

Rui Wang [1], Heather A. Owen [2] and Anna A. Dobritsa [1,*,†]

1 Department of Molecular Genetics and Center for Applied Plant Sciences, Ohio State University, Columbus, Ohio 43210, USA
2 Department of Biological Sciences, University of Wisconsin, Milwaukee, Wisconsin 53211, USA

*Author for communication: dobritsa.1@osu.edu
†Senior author.

R.W., H.A.O., and A.A.D. conceived and designed the experiments. R.W. and H.A.O. performed the experiments. R.W., H.A.O., and A.A.D. analyzed the data and wrote the article.

The author responsible for distribution of materials integral to the findings presented in this article in accordance with the policy described in the Instructions for Authors (https://academic.oup.com/plphys/pages/General-Instructions) is Anna A. Dobritsa (dobritsa.1@osu.edu).

Abstract

Formation of pollen wall exine is preceded by the development of several transient layers of extracellular materials deposited on the surface of developing pollen grains. One such layer is primexine (PE), a thin, ephemeral structure that is present only for a short period of time and is difficult to visualize and study. Recent genetic studies suggested that PE is a key factor in the formation of exine, making it critical to understand its composition and the dynamics of its formation. In this study, we used high-pressure frozen/freeze-substituted samples of developing Arabidopsis (*Arabidopsis thaliana*) pollen for a detailed transmission electron microscopy analysis of the PE ultrastructure throughout the tetrad stage of pollen development. We also analyzed anthers from wild-type Arabidopsis and three mutants defective in PE formation by immunofluorescence, carefully tracing several carbohydrate epitopes in PE and nearby anther tissues during the tetrad and the early free-microspore stages. Our analyses revealed likely sites where these carbohydrates are produced and showed that the distribution of these carbohydrates in PE changes significantly during the tetrad stage. We also identified tools for staging tetrads and demonstrate that components of PE undergo changes resembling phase separation. Our results indicate that PE behaves like a much more dynamic structure than has been previously appreciated and clearly show that Arabidopsis PE creates a scaffolding pattern for formation of reticulate exine.

Introduction

Pollen grains are protected by a complex, multi-layered pollen wall. Exine, the outer layer of the pollen wall, is particularly remarkable. It is composed of an unusual biopolymer, sporopollenin, assembling on the pollen surface into intricate, and diverse species-specific patterns (Ariizumi and Toriyama, 2011). Unlike other plant cell walls, produced by the cells they will eventually cover, exine is formed through an unusual partnership between microspores (cells of male reproductive lineage developing into pollen grains) and the nearby sporophytic layer of tapetum (Ariizumi and Toriyama, 2011; Wang and Dobritsa, 2018). Tapetum synthesizes most sporopollenin precursors and possibly other components required for exine formation, which are then transported to the surface of microspores to assemble into exine or create conditions for its assembly. Microspores likely also produce some materials for exine formation, although their role in this process is less clear.

The general order of events during the exine formation is well defined (Heslop-Harrison, 1968; Owen and Makaroff,

Received June 07, 2021. Accepted August 08, 2021. Advance access publication September 14, 2021

1995; Ariizumi and Toriyama, 2011; Quilichini et al., 2014). The process begins at the tetrad stage of pollen development when clusters of four sister microspores generated via meiosis by the microspore mother cell (MMC) are temporarily kept together under the protective layers of the callose wall (CW) and the MMC primary cell wall overlying the CW. During the tetrad stage, the plasma membrane (PM) of each microspore starts separating from the CW, forming undulations. Around the same time, a thin layer of extracellular matrix, known as primexine (PE), forms between the microspore PM and the CW. PE is thought to serve as a scaffold for the formation of the incipient exine elements, probaculae, and protectum, which appear within the PE matrix at the late tetrad stage and may contain early sporopollenin (Heslop-Harrison, 1968). At the end of the tetrad stage, the CW is dissolved and free unicellular microspores are released into the anther locule. During the free-microspore stage, PE gradually disappears, while the thin probaculae and protectum become, respectively, transformed into more massive column-like baculae and roof-like tectum, the sporopollenin-based elements of the mature exine.

Although this sequence of events seems to be fairly consistent across species (Blackmore et al., 2007; Ariizumi and Toriyama, 2011; Shi et al., 2015; Wang and Dobritsa, 2018; Gabarayeva and Grigorjeva, 2021), the contribution of PE to this process remains unclear. Genetic studies in Arabidopsis (*Arabidopsis thaliana*) and rice (*Oryza sativa*) confirm the importance of PE to exine development. In multiple mutants of these species, PE defects are strongly associated with the inability to form normal exine and, often, with pollen lethality (Paxson-Sowders et al., 2001; Ariizumi et al., 2004; Guan et al., 2008; Chang et al., 2012; Li et al., 2020; Mondol et al., 2020; Xu et al., 2020). Yet, there is little direct evidence to support the hypothesis that PE acts as an exine scaffold.

Given the importance of PE to the formation of exine, it is critical to understand its structure and composition. Yet, PE has been challenging to characterize. The tetrad stage is one of the briefest in pollen development and, correspondingly, hard to identify and capture: only one or two floral buds in a typical Arabidopsis inflorescence have microspores at this stage. Thus, there are no transcriptomic/proteomic studies of this stage. Biochemical analysis of PE is also a challenge, due to scarcity of material and its inaccessible position under other extracellular layers. In addition, occupying a narrow space of ~100 nm between the microspore PM and the CW, PE is hard to visualize. While high-resolution transmission electron microscopy (TEM) has been used as the primary approach to see PE, the relatively low electron density of this structure, the challenge of obtaining pollen at this stage, and the fact that TEM—especially in chemically fixed samples—is often prone to artifacts, make it difficult to carefully observe PE throughout the duration of the tetrad stage and compare results obtained by different groups. With few exceptions (e.g. Fitzgerald and Knox, 1995; Paxson-Sowders et al., 2001; Quilichini et al., 2014; Gabarayeva and Grigorjeva, 2021), most publications on exine formation have resorted to providing a single image of PE-containing tetrad-stage microspores, potentially missing brief but critical events occurring at this stage or inadvertently comparing samples collected at different developmental moments.

Despite these challenges, some ideas about PE have emerged. While its exact composition is unknown, PE is thought to contain polymeric carbohydrates, such as cellulose and pectin (Heslop-Harrison, 1968; Rhee and Somerville, 1998; Majewska-Sawka and Rodriguez-Garcia, 2006). Recent studies of Arabidopsis mutants have suggested that xylan and arabinogalactans might also serve as components of PE (Li et al., 2017; Suzuki et al., 2017). Biophysical modeling of exine patterning and attempts to recapitulate exine formation in vitro suggested that, to create proper conditions for exine patterning, components of PE may undergo phase separation (Radja et al., 2019; Gabarayeva and Grigorjeva, 2021). TEM studies of PE in chemically fixed samples from purple passionflower (*Passiflora incarnata*) and Carolina allspice (*Calycanthus floridus*) were consistent with phase separation (Radja et al., 2019; Gabarayeva and Grigorjeva, 2021), although the details of this process and its universality remained unclear.

Here, we present a systematic analysis of PE throughout the tetrad stage of development, reconstructing the sequence of events associated with this transient layer in Arabidopsis, the primary model organism for molecular-genetic studies of exine formation. Our goals were (1) to determine if PE undergoes changes in its structure and composition as the tetrad-stage progresses, including changes indicative of phase separation and (2) to define characteristic components that can serve as temporal landmarks for different substages of the tetrad stage. To this end, we performed TEM analysis of PE in high-pressure frozen/freeze-substituted samples and used immunofluorescence microscopy to carefully trace several carbohydrate epitopes in PE and surrounding tissues during the tetrad stage of pollen development in wild-type and several PE mutants. Our study revealed a much more dynamic picture of PE than previously appreciated and identified temporal landmarks and probes that will be useful for future analyses of this structure.

Results and discussion

TEM analysis of microspores at the tetrad stage reveals distinct changes in the PE ultrastructure

To better understand the events happening in PE, we focused specifically on the tetrad stage of Arabidopsis pollen development and examined the ultrastructure of PE throughout this stage using TEM. To preserve this delicate layer and avoid artifacts commonly associated with chemical fixation, we prepared samples using rapid high-pressure freezing followed by freeze substitution. TEM was done on

Columbia-0 (Col-0), *inaperturate pollen1* (*inp1-1*), and *large and square pollen6* (*lsq6*) plants, which, while differing in pollen aperture patterns, have identical reticulate exine patterns (Dobritsa et al., 2011). Exine and PE are thicker in tetraploid *lsq6* than in the other two diploid genotypes, making its PE easier to visualize, yet no differences in the process of PE formation were noticed between the three genotypes. In total, tetrads from 44 anthers were examined (8 wild-type Col-0, 13 *lsq6*, and 23 *inp1*), spanning the duration of the tetrad stage and, when combined, allowing us to reconstruct the order of events within the PE layer.

At the early tetrad stage, microspore PM was in direct contact with the CW and only a few small tufts of PE appeared at regular intervals between the PM and the CW (Figure 1A; see also Figure 1J for the interpretation of all TEM images). When a thin PE layer became visible between the PM and the CW, it initially had homogeneous structure and uniform, light-gray, electron density (Figure 1B). No PM undulations were visible at that point. Later, PE became less homogeneous, with regions of higher electron density appearing within it. Although, at first, these regions were barely visible (Figure 1C), they became much more prominent in (presumably) slightly older microspores, with PE developing a clear periodic pattern of lighter and darker regions (Figure 1D). Eventually, the microspore PM developed an undulating pattern, with the prominent dark regions of PE overlying the troughs of the PM and likely pushing the PM inward (Figure 1E). These regions seem equivalent to the so-called "spacers" noticed in some earlier studies of PE (Fitzgerald and Knox, 1995; Quilichini et al., 2014). This was followed by the apparent unmixing of two phases in PE (Figure 1F) and, eventually, the appearance of electron-dense probaculae and protectum, predecessors of the future exine elements (Figure 1G). In all cases where probaculae/protectum were not fully formed, the protectum appeared more developed than the probaculae, suggesting that the growth of these structures occurs from the top of PE toward the PM. Finally, in microspores with well-developed probaculae and protectum, PE displayed clear signs of periodic phase separation, with two phases of different electron density visible in this layer (Figure 1H; Supplemental Figure S1). We refer to this stage as the "Golden Gate" stage, as the arrangement of probaculae and the two PE phases resembles the silhouette of the eponymous bridge. At this stage, positions of probaculae/protectum coincided with the more electron-dense phase of PE (resembling, respectively, the towers and the main cables of the bridge), while the less electron-dense phase occupied the regions between the incipient exine elements (Figure 1, H and J; Supplemental Figure S1). While the "Golden Gate" pattern of phase separation was most easily seen in the thicker PE of diploid *lsq6* microspores (Figure 1H), it was also observed in haploid microspores of *inp1-1* (Supplemental Figure S1, A–D), as well as in haploid microspores of another wild-type accession, Wassilewskija (Ws), whose samples were prepared similarly yet separately (Supplemental Figure S1E). A tangential section through an *inp1-1* microspore at this stage clearly demonstrated that PE itself becomes organized into a mesh-like pattern, matching the reticulate exine pattern in mature Arabidopsis pollen (Figure 1I). This shows that the arrangement of the two phases of PE can indeed create a scaffold for the developing exine elements.

Xylan content in PE and in nearby cells changes dynamically during the tetrad stage

Our TEM analysis shows that PE undergoes clear changes in its ultrastructure as the tetrad stage progresses. This is likely due to changes in its chemical content, making it important to understand how the composition of PE changes throughout the tetrad stage. To answer this question, we prepared sections of 12 tetrad-containing buds collected from 7 wild-type Arabidopsis plants and stained them with monoclonal antibodies (mAbs) against several carbohydrates previously proposed as possible PE components. We also stained all sections with Calcofluor White, which stains cellulose and callose (Bidhendi et al., 2020), allowing us to see the CW around the developing pollen and cell walls of other anther layers (except for tapetum, whose walls lack cellulose at that point). Since, in Arabidopsis, pollen development in different anthers of the same bud and even different locules of the same anther is not perfectly synchronous, we assessed these 12 buds for the presence of pollen stages other than tetrads (Supplemental Figure S2). This allowed us to assign tetrads from each bud to the "early," "middle," or "late" substages (Supplemental Table S1). For example, tetrads from a bud that also contained MMCs would be at a younger stage than tetrads from a tetrads-only bud, which, in turn, would be younger than tetrads from a bud that also contained released microspores.

Recent genetic analysis in Arabidopsis suggested that xylan could be one of the components of PE, although that study suggested it is not present until after tetrad dissolution (Li et al., 2017). To investigate xylan content in PE, we used the LM11 and LM10 mAbs (McCartney et al., 2005) and found that the xylan epitopes they recognize were clearly present in PE during the tetrad stage (Figure 2; Supplemental Figures S3 and S4). Besides microspores (and tapetum in the case of LM11—see below), no other anther cell layers were stained with these antibodies.

LM11 revealed a particularly dynamic pattern of changes in xylan in PE and in surrounding cells (Figure 2; Supplemental Figure S3). In early tetrads, punctate LM11 signal was present both on the microspore surface (i.e. at the position of PE) and inside the microspores, suggesting that at this stage microspores produce xylan for PE. In middle- and late-stage tetrads, LM11 signal in PE became continuous, while the signal inside microspores disappeared. At the late stage, puncta of LM11 signal also appeared in the anther locules, and later, at the tetrad-dissolution and early free-microspore stages, massive amounts of LM11 epitopes were present both inside the locules and in tapetum,

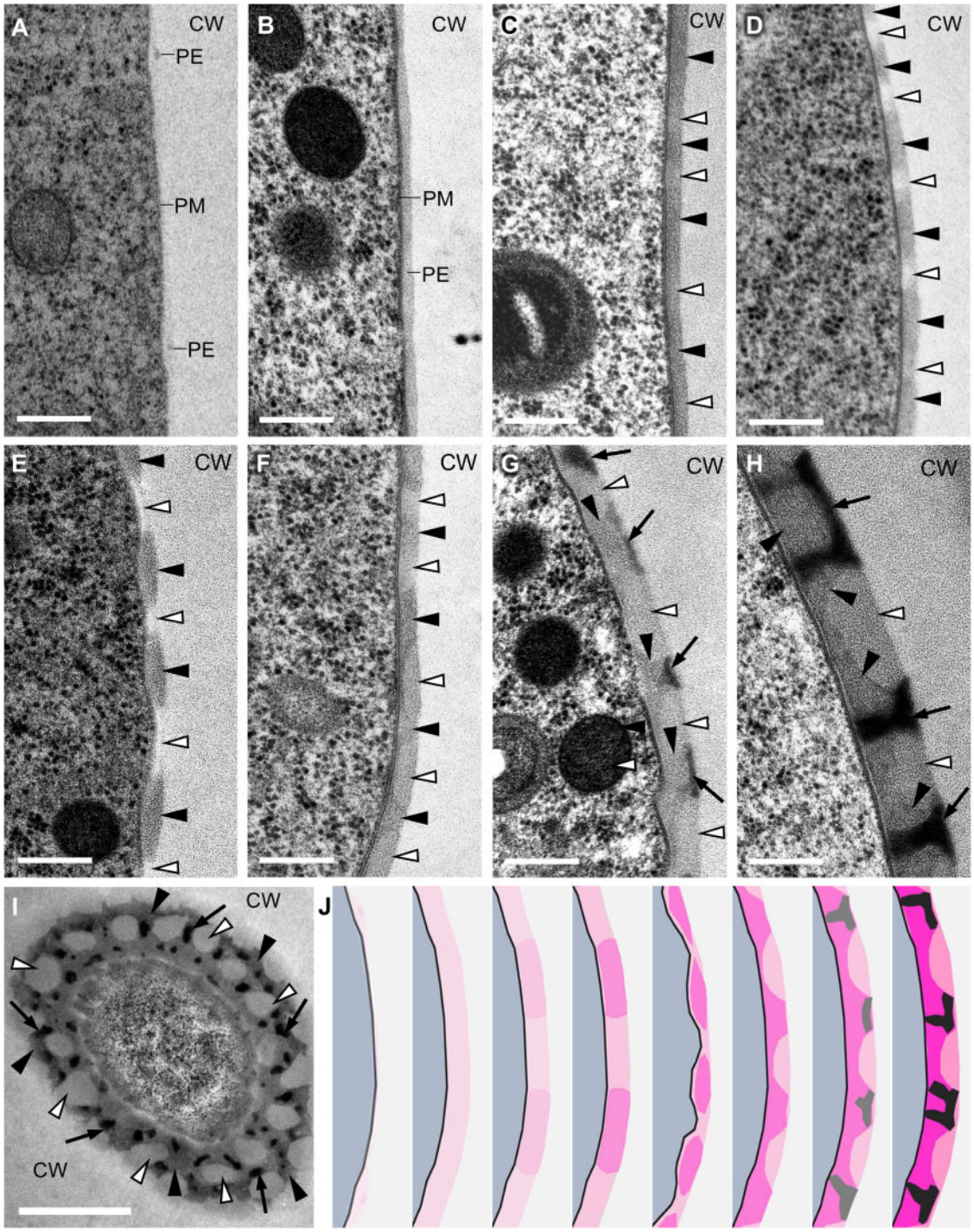

Figure 1 PE formation during the tetrad stage leads to phase separation and creates reticulate scaffold for incipient exine elements. A–I, Transmission electron micrographs of sections through microspores at different points during the tetrad stage of development. White arrowheads indicate light regions of PE. Black arrowheads indicate dark regions of PE. Black arrows indicate developing probaculae/protectum. Images (B–F) are from Col-0; images (A), (G), and (I) are from *inp1*; image (H) is from *lsq6*. Scale bars = 250 nm in (A–H) and 1 μm in (I). A, At the early tetrad stage, microspore PM directly opposes the CW and only a few tufts of PE appear between the PM and the CW. B, A thin layer of PE develops between the PM and the CW. C, Periodic light and dark regions appear within the PE. D, The separation of PE into light and dark regions becomes obvious. E, PM undulates under the PE, with darker regions of PE corresponding to the troughs in PM. F, Phase separation within PE creates menisci of light phase separated from the dark phase. G, Incipient exine elements (protectum, in particular) start forming within the dark-phase regions. H, The "Golden Gate" stage, with clear light and dark phases of the PE and with protectum and probaculae forming within the dark-phase regions. This image is from a diploid *lsq6* microspore that has thicker PE than haploid microspores, making the structural details more visible. Similar structures were also observed in haploid microspores at the same stage (see Supplemental Figure S1). I, A tangential cross section through a microspore at the "Golden Gate" stage showing clear reticulate pattern of PE. J, A schematic summary of events happening at the microspore periphery during the tetrad stage of development, with the two PE phases represented by the light and dark shades of pink and probaculae/protectum shown in black.

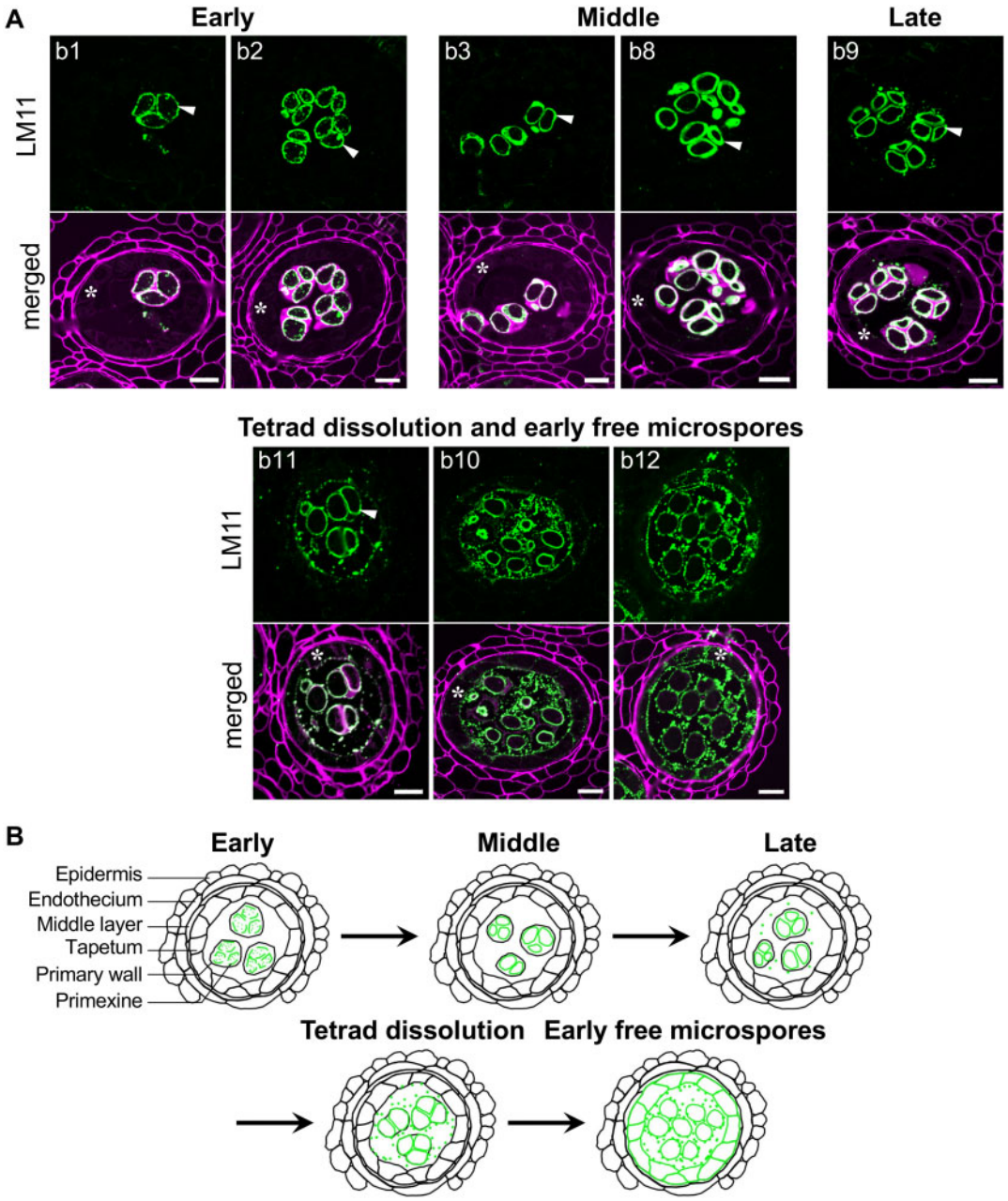

Figure 2 Distribution of the LM11 xylan epitope in wild-type anthers changes dynamically during the tetrad stage of pollen development. A, Images from representative buds at different substages of the tetrad stage and soon after the tetrad dissolution. See Supplemental Figure S3 for images from all 12 buds. Green, LM11 signal; magenta, Calcofluor White signal. Signal in PE is indicated by white arrowheads. Tapetum is indicated by asterisks. Scale bars = 10 μm. B, A diagram of changes in the distribution of the LM11 epitope in tetrad-stage anthers.

suggesting that toward the end of the tetrad stage the site of xylan production switches from microspores to tapetum.

The xylan epitope recognized by LM10 was also present in PE, although the LM10 signal was consistently weaker than the LM11 signal (Supplemental Figure S4). The LM10 epitope showed only a punctate pattern throughout the tetrad stage, never forming a continuous signal in PE. This indicates that the xylan epitopes recognized by the two antibodies likely differ in their placement within the PE. While both mAbs can bind the unsubstituted xylan backbone, LM11 also binds strongly to more substituted xylans, such as arabinoxylan (McCartney et al., 2005), suggesting that most of the xylan in PE is likely substituted.

Dynamic changes during the tetrad stage also occur in pectins in PE and surrounding tissues

In addition to xylan, pectin was also reported in PE (Rhee and Somerville, 1998; Aouali et al., 2001; Majewska-Sawka and Rodriguez-Garcia, 2006). We, therefore, used the JIM7 and JIM5 mAbs, recognizing, respectively, pectin homogalacturonans with high (HME) and low (LME) degrees of methylesterification (Clausen et al., 2003). The two antibodies

revealed somewhat different but, in both cases, dynamic changes in the content of their respective epitopes in the anther tissues.

At the early tetrad stage, JIM7 stained cell walls in all anther layers, including tapetum and the primary cell wall surrounding tetrads (the remnant of the MMC cell wall) (Figure 3; Supplemental Figure S5). Yet, there was no JIM7 signal on the surface of microspores, indicating that there is no HME pectin in early tetrad PE. In middle-stage tetrads, however, some punctate JIM7 signal appeared inside microspores and a continuous signal emerged in the PE. After appearing in PE at the middle-tetrad stage, the JIM7 signal remained there for the duration of the tetrad stage and after microspore release. Notably, at the late tetrad stage, the JIM7 signal disappeared from two sites—the tapetal cell walls and tetrad primary cell walls (Figure 3; Supplemental Figure S5). This likely removes some barriers surrounding tapetum and tetrads in preparation for active tapetal secretion and massive sporopollenin deposition. The characteristic dynamics of changes in the JIM7 pattern in tapetum, PE, and the primary cell wall of tetrads suggest that JIM7 would provide an excellent probe for staging tetrads.

Unlike JIM7, JIM5 showed very little reactivity in early tetrad-stage anthers (Figure 4; Supplemental Figure S6). The only signal at this stage was exclusively in the cells of the anther middle layer facing the neighboring locules. However, at the middle-tetrad stage, a punctate JIM5 signal appeared in the PE and inside the microspores (Figure 4; Supplemental Figure S6), indicating both HME and LME pectins accumulate at this stage in the PE. The use of JIM5 and JIM7 on the same locules allowed us to conclude that the JIM5 signal appears in PE slightly later than the JIM7 signal. This is consistent with pectin, initially synthesized in an HME form (Mohnen, 2008), undergoing de-esterification in PE by pectin methylesterases. At the late tetrad stage, the initially weak punctate JIM5 signal in PE was replaced by a strong and continuous signal, which remained there through the tetrad dissolution and the early free-microspore stage (Figure 4; Supplemental Figure S6). Additionally, JIM5-positive puncta appeared at the late stage inside the tapetal cells. Thus, the LME pectin becomes a prominent feature of PE at later stages. Since such compositional changes can increase pectin's ability to undergo cleavage (Willats et al., 2001), this might indicate softening of PE. However, in some systems, the de-methylesterified pectins can, via cross-linking with Ca^{2+} ions, increase cell wall stiffness (Willats et al., 2001). Further investigations will be required to probe exactly how properties of PE are affected by pectin de-methylesterification at the end of the tetrad stage.

No detectable arabinogalactan moieties are present in PE of tetrad-stage microspores

We also used the JIM8 and JIM15 mAbs (Pattathil et al., 2010) on tetrad-containing anthers to investigate the presence of arabinogalactans, also proposed to be a part of PE (Suzuki et al., 2017). Both antibodies produced strong signals in the primary cell walls of tetrads at the early- and middle-tetrad stages; this signal disappeared at the late-tetrad stage. However, in PE, no convincing signal was observed at any stage (Supplemental Figures S7 and S8). Other anti-arabinogalactan mAbs (JIM4, JIM13, JIM17, JIM20, and MAC207), tested on a more limited number of buds, also failed to produce signals in the PE of the tetrad-stage microspores.

Immunofluorescence analysis of PE composition in three PE mutants

After establishing how xylan and the two types of pectin change in wild-type anthers, we used the LM11, JIM5, and JIM7 mAbs to investigate the PE composition of three mutants previously suspected to have abnormal PE formation.

The first was a double mutant with the defects in *SPONGY2/IRREGULAR XYLEM9-LIKE* (*SPG2/IRX9L*) and *IRX14L*, predicted to encode glycosyl transferases required for the elongation of the β-1-4-xylan backbone. Single mutations in these genes lead to abnormalities in exine patterning (Dobritsa et al., 2011; Li et al., 2017), and earlier analysis of PE in the *spg2* mutant hinted at a defect in xylan content (Li et al., 2017).

We used LM11 on sections of four *spg2 irx9l* buds with tetrads at approximate early-to-middle and middle stages (Supplemental Figure S9; Supplemental Table S2). Although at the middle stage of development wild-type tetrads show clear continuous LM11 signal in PE (Figure 2), tetrads from all four *spg2 irx14l* buds showed only punctate staining (Figure 5A), demonstrating that xylan does not accumulate in the *spg2 irx14l* PE normally. Similarly, no pectin signal was found in the *spg2 irx14l* PE with either JIM7 or JIM5 mAbs (Supplemental Figure S10). This result underscored the importance of proper tetrad staging. The oldest tetrads in this case came from the tetrad-only buds which still showed the JIM7 signal in their tapetal walls and the primary cell walls of tetrads (Supplemental Figure S10), indicating they have not yet reached the late-tetrad stage and could have been too young to produce a clear JIM5 signal in PE. Still, they should have been at the appropriate stage for the JIM7 PE signal. The absence of this signal indicates pectin deposition is likely also affected in the *spg2 irx14l* PE.

We also assessed PE composition in *no PM undulation* (*npu*) and *ruptured pollen grain1* (*rpg1*) mutants. In both mutants, defects in exine deposition and associated pollen lethality were hypothesized to be caused by defects in PE, but the roles of these genes in exine formation remain unclear. In *npu*, PE was reported absent (Chang et al., 2012), while *rpg1* was described as having irregular PE, although no additional details about its defects were provided (Guan et al., 2008). For *npu*, we obtained tetrads from four buds from middle to late stages of development and for *rpg1*, tetrads from three buds at the early, middle-to-late, and late stages (Supplemental Figures S11 and S12; Supplemental Table S2).

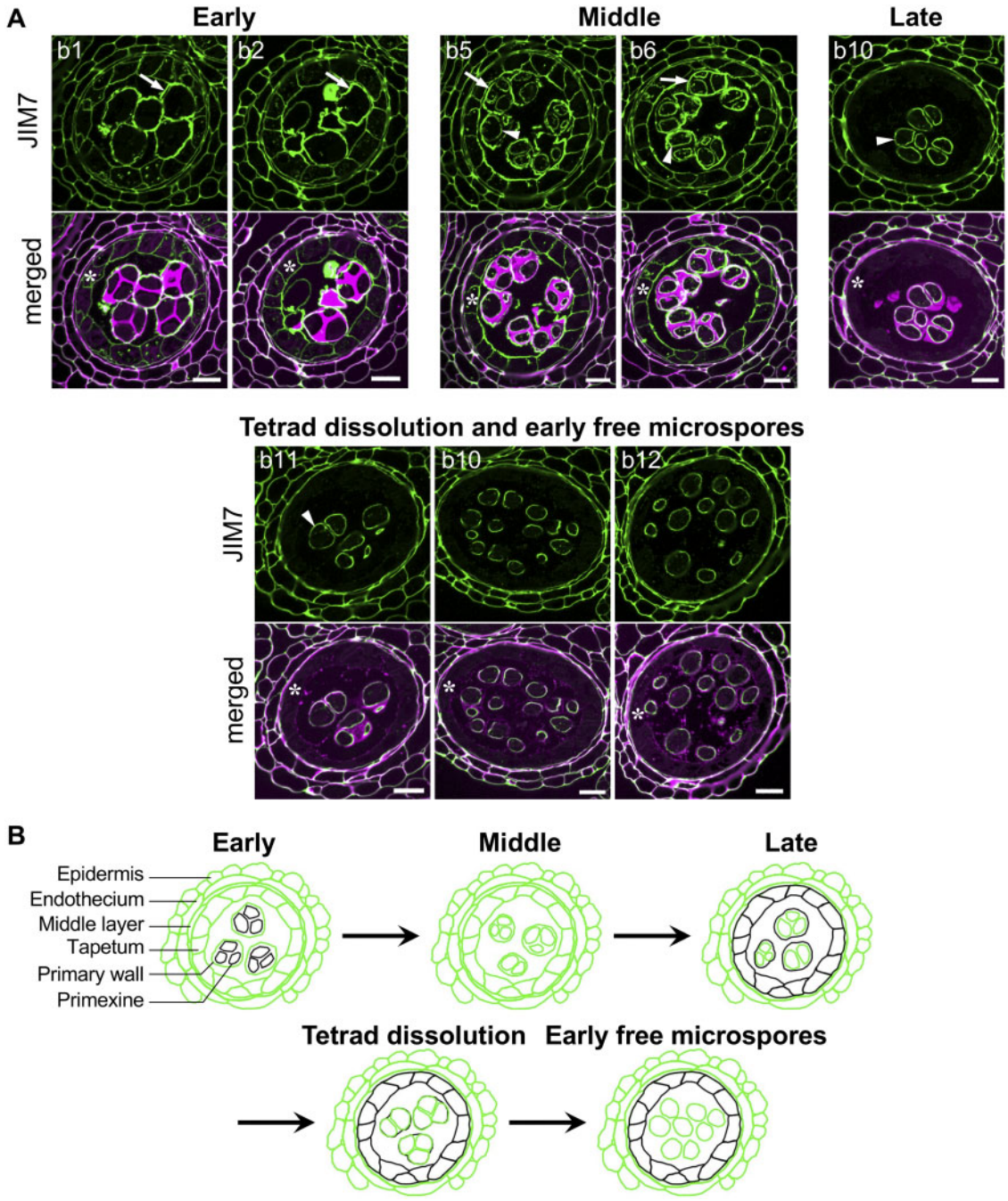

Figure 3 Distribution of the JIM7 highly methylesterified pectin epitope in wild-type anthers changes dynamically during the tetrad stage of pollen development. A, Images from representative buds at different substages of the tetrad stage and soon after the tetrad dissolution. See Supplemental Figure S5 for images from all 12 buds. Green, JIM7 signal; magenta, Calcofluor White signal. Signal in PE is indicated by white arrowheads. Signal in the primary cell wall is indicated by white arrows. Tapetum is indicated by asterisks. Scale bars = 10 μm. B, A diagram of changes in the distribution of the JIM7 epitope in tetrad-stage anthers.

Consistent with the previously proposed lack of PE, *npu* tetrads exhibited significant defects in the antibody staining of PE (Figure 5, B–D). When stained with LM11, even though the *npu* PE displayed a punctate signal characteristic of the early tetrads, it failed to develop the continuous signal expected of the later stages analyzed here (Figure 5B). In addition, no pectin signal appeared in the *npu* PE at any stage with either JIM7 or JIM5 (Figure 5, C and D). Thus, the *npu* tetrads fail to deposit xylan and both types of pectin on the microspore surface, confirming substantial defects in PE formation in this mutant. Except for PE, the characteristic JIM7 patterns were normal in the *npu* cell walls and changed consistently with the age of tetrads (Figure 5C), confirming that the JIM7 pattern can serve as a reliable indicator of the tetrad substages and demonstrating the specificity in the loss of the PE signal in *npu*. On some occasions,

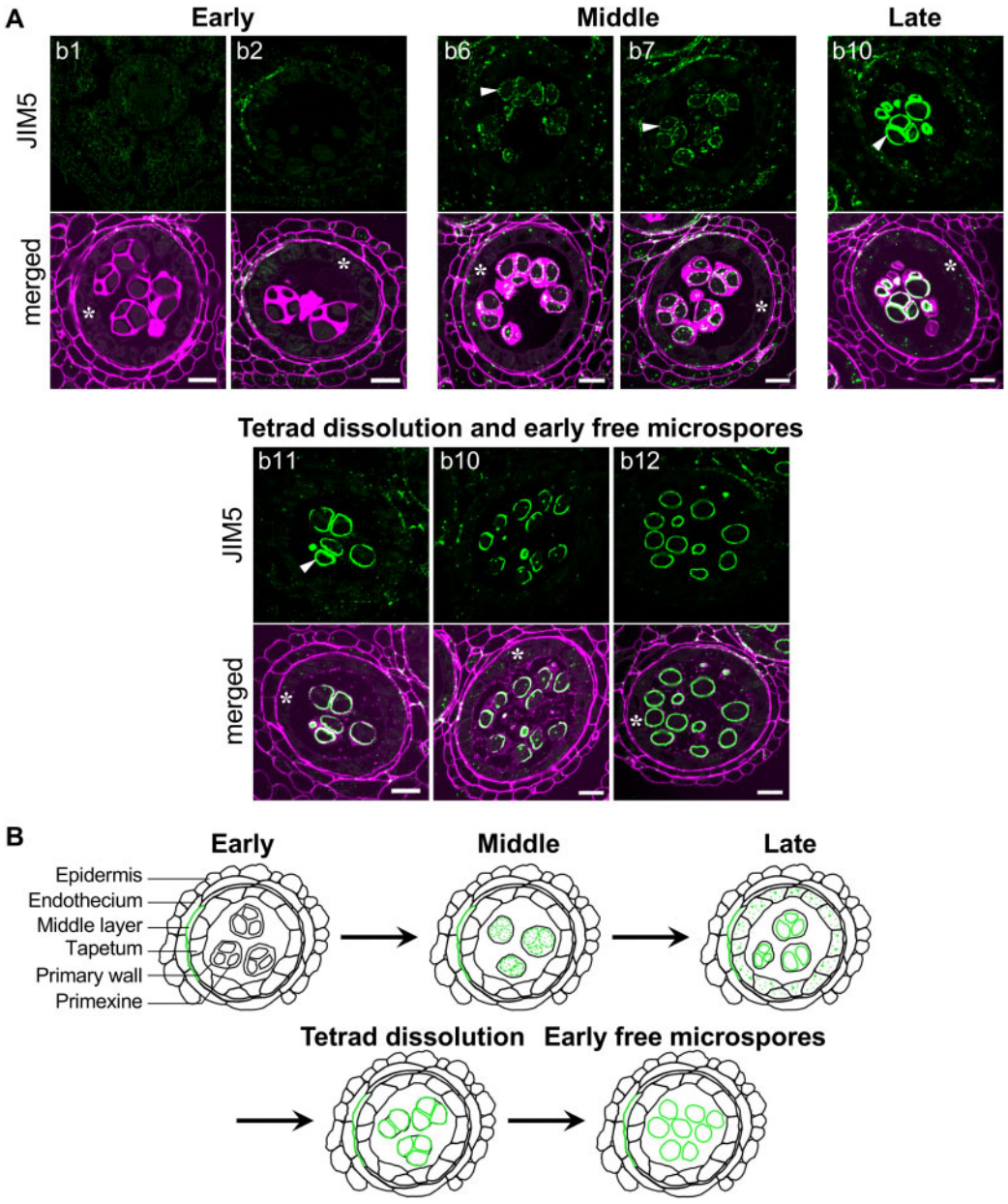

Figure 4 Distribution of JIM5 low-methylesterified pectin epitope in wild-type anthers changes dynamically during the tetrad stage of pollen development. A, Images from representative buds at different substages of the tetrad stage and soon after the tetrad dissolution. See Supplemental Figure S6 for images from all 12 buds. Green, JIM5 signal; magenta, Calcofluor White signal. Signal in PE is indicated by white arrowheads. Tapetum is indicated by asterisks. Scale bars = 10 μm. B, A diagram of changes in the distribution of the JIM5 epitope in tetrad-stage anthers.

JIM5 produced strong signal in the primary cell walls of the *npu* tetrads (Figure 5D, bud b3). As such signal was never observed in this layer in wild-type tetrads, it is possible that the primary cell wall of the *npu* tetrads also has differences in its pectin composition.

In contrast to *npu*, *rpg1* PE appeared to have minor defects, if any, in its xylan and pectin composition (Supplemental Figure S13). The LM11 and JIM7 signals were normal in the *rpg1* tetrads, whereas the JIM5 signal, although slow to develop (as late-stage *rpg1* tetrads still failed to produce a clear signal), appeared normal in released microspores.

Conclusions

Altogether, our results demonstrate that PE in developing Arabidopsis microspores behaves as a highly dynamic layer that changes its xylan and pectin composition and modifies its ultrastructure throughout the tetrad stage of development, ultimately creating distinct phases of higher and lower electron density. At the late tetrad stage, these phases become organized in a pattern that provides a scaffold for the development of exine elements, allowing them to assemble into a reticulate pattern. Our findings also suggest that, in the future, care should be taken when comparing different samples to

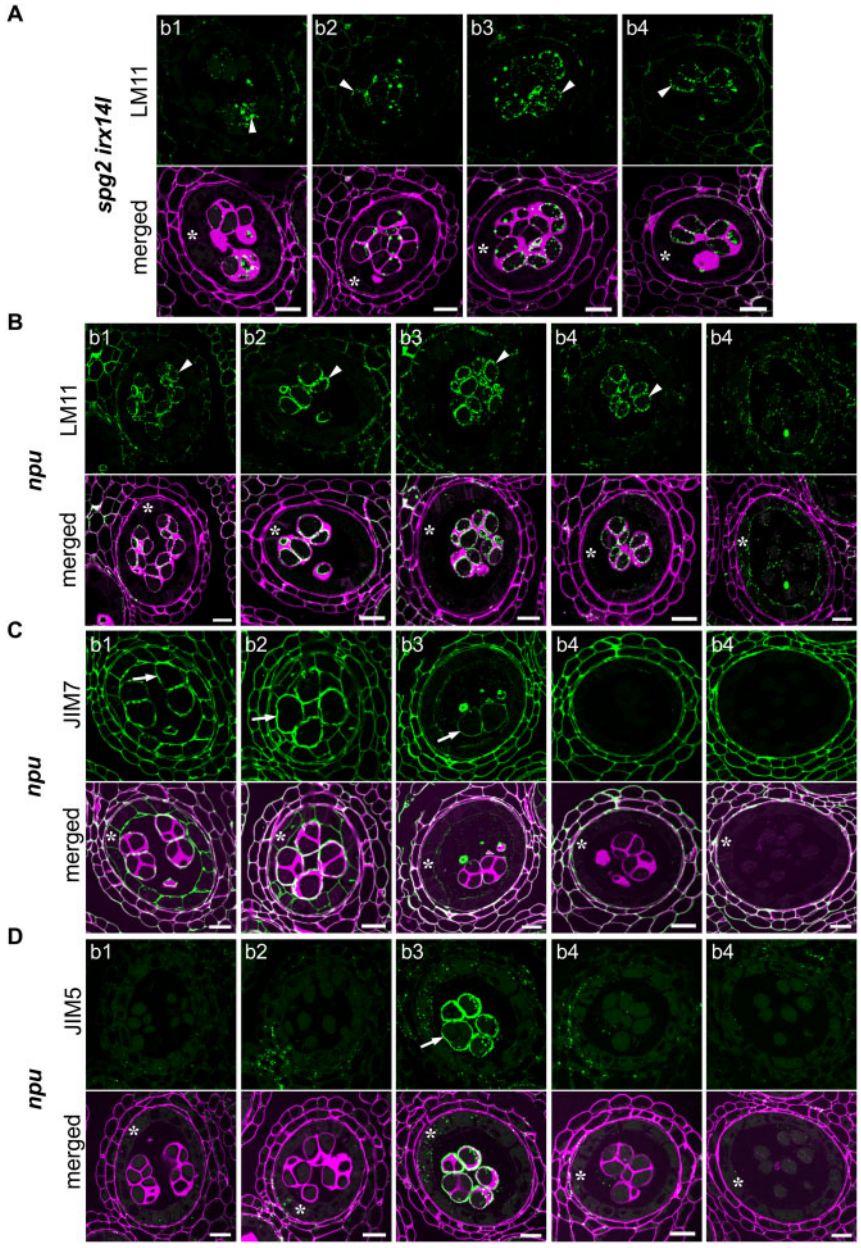

Figure 5 Distribution of the LM11 xylan, JIM7 highly methylesterified pectin, and JIM5 low-methylesterified pectin epitopes in tetrad-containing anthers of *spg2 irx14l* and *npu* mutants. Green, signals from indicated anti-carbohydrate antibodies; magenta, Calcofluor White signal. Signal in PE is indicated by white arrowheads. Signal in the primary cell wall is indicated by white arrows. Tapetum is indicated by asterisks. Scale bars = 10 μm. Compare with wild-type anthers in Figures 2–4.

properly stage tetrads and that JIM7 provides a convenient staging tool.

Materials and methods

Plant material and growth conditions

Arabidopsis (*A. thaliana*) plants of the following genotypes were used: wild-type Col-0, *inp1-1* (Dobritsa et al., 2011), *lsq6* (Dobritsa et al., 2011), double mutant *spg2/irx9l* (SALK_037323) *irx14l* (SALK_066961), *npu-2* (Salk_062174), and *rpg1-1* (Salk_142803). Plants were grown at 22°C under the 16-h light/8-h dark cycle in growth chambers at the OSU Biotechnology greenhouse with F96T12 fluorescent lamps and 60-W incandescent bulbs providing the 120–150 μmol m^{-2} s^{-1} white light, or at UW-Milwaukee in a Percival AR66L Arabidopsis chamber with FO17/741 Eco fluorescent lamps and 25-W incandescent bulbs providing 100–125 μmol m^{-2} s^{-1} white light.

High-pressure freezing and freeze substitution

On days when high-pressure freezing was performed, plants were removed from the growth chamber at UW-Milwaukee and placed into a Rubbermaid chest cooler (Model 1848).

To maintain humidity, pot-holding trays were placed onto a layer of wet cellulose sponges, then transported to University of Wisconsin-Madison by car (~1.5–h trip). Flower buds of appropriate sizes were dissected under stereomicroscopes in drops of 0.1 M sucrose. A single anther was removed from each bud, placed onto a microscope slide in a drop of sucrose solution, squashed under a coverslip, and examined with a compound microscope. When tetrads were present, the rest of the bud was placed into the depression of a Pelco Type B freezer hat (Ted Pella, 39201) pre-coated with 3% (w/v) lecithin in chloroform and containing 0.1 M sucrose (Kiss and Staehelin, 1995). A freezer hat (planchet) with multiple buds was placed into the sample holder of a high-pressure freezer (ABRA Fluid AG Model HPM 010), and a second Type B hat was placed on top of it, flat side down. Planchets were frozen with the high-pressure freezer, then removed from the sample holder under liquid nitrogen (LN_2), placed into cryovials in LN_2, snapped into canes, transferred into a Taylor Wharton CP 30 cryogenic shipper, and transported to UW-Milwaukee.

Frozen material was freeze-substituted in 2% (w/v) OsO_4 in acetone using a Leica AFS. Cryovials with freeze-substitution medium were frozen in LN_2 and placed into the chamber of the cooled AFS. Planchets with frozen material were placed on top of the solid freeze-substitution media, cryovials were sealed, and the first program was started (T1 = −100°C, 1 h; S1 = +5°C, 2 h; T2 = −90°C, 168 h; S2 = +5°C, 14 h; T3 = −20°C, 4 h), followed by the second program (T1 = −20°C, 0.1 h; S1 = +4°C, 6 h; T2 = 4°C, 2 h; S2 = +8°C, 0.5 h; T3 = 8°C, 1 h). The cryovials were then removed and kept at room temperature for 2 h, and the solution in cryovials was replaced with anhydrous acetone (five changes, 5 min each). Contents of cryovials with the same genotype were pooled into a glass dish, and individual anthers were transferred with Pasteur pipet under a stereomicroscope into a 1-dram glass shell vial containing anhydrous acetone. Anthers were then infiltrated with modified Spurr's resin in anhydrous acetone (Holdorf et al., 2012) without accelerator, according to the schedule adapted from (Kang, 2010): 5% (v/v) resin, overnight; 10% (v/v) resin, 4 h; 20% (v/v) resin, 4 h; 40% (v/v) resin, minimum of 4 h; 60% (v/v) resin, minimum of 4 h; 80% (v/v) resin, minimum of 4 h; 100% resin, 48 h. Several changes were then made every 24 h into 100% resin with accelerator, prepared fresh every day. Following infiltration, individual anthers were placed into 21-cavity EM embedding molds (Ted Pella, #10505), oriented for cross-sectioning, and polymerized for 48 h at 60°C.

TEM

Pale gold sections were cut using a Reichert-Jung Ultracut E ultramicrotome, placed onto 200 or 400 mesh copper grids, stained with 2% (w/v) uranyl acetate in 70% (v/v) methanol, followed by Reynold's Lead Citrate. Sections were examined with a Hitachi H-600 transmission electron microscope operating at 75 kV. Images were captured with Kodak 4489 film, developed, and scanned at 2,000 dpi using an Epson Perfection V750 Pro scanner to obtain digital images. Tetrads from 44 anthers were examined (8 wild-type Col-0, 13 *lsq6*, and 23 *inp1*).

Immunofluorescence labeling

Main inflorescences of Arabidopsis 1 week after bolting were fixed in 2.5% (v/v) glutaraldehyde, 1% (v/v) Triton X-100, 0.1 M HEPES, pH 7.2, and flower buds from each inflorescence were individually embedded in LR White resin (Hard grade; Ted Pella). The inflorescence fixation, bud embedding, sectioning, immunofluorescent labeling, and imaging were performed as previously described (Wang and Dobritsa, 2021). Tetrad-containing buds were first identified with brightfield microscopy on toluidine blue-stained cross-sections and confirmed by Calcofluor White (0.02% (w/v)) staining and confocal microscopy. The rat LM10 and LM11 mAbs (Megazyme, Bray, Ireland) were used at 1:100 dilution. The rat JIM4, JIM5, JIM7, JIM8, JIM13, JIM15, JIM17, JIM20, and MAC207 mAbs (CarboSource Service, Athens, GA, USA) were used at 1:40 dilution. The secondary antibody (goat anti-rat-Alexa 488; Thermo Fisher, Waltham, MA, USA) was used at 1:100 dilution. Sections were examined with Nikon A1+ confocal microscope (100× objective, NA = 1.45). Alexa 488 and Calcofluor White were sequentially excited by the 488 and 405 nm lasers, and signals were collected separately at 500–550 nm (Alexa 488) and 450 nm (Calcofluor White). The parameters of laser power and high voltage (gain) were set up, respectively, at 10% and 140 for LM10; 5%–10% and 85–120 for LM11; 10% and 120 for JIM5; 10% and 90 for JIM7; 10% and 125 for JIM8; 10% and 120–125 for JIM15, and 10% and 80–90 for Calcofluor White. Experiments were repeated 3 times, with similar results.

Accession numbers

The Arabidopsis Genome Initiative accession numbers for the genes used in this study are the following: At1g27600 (*SPG2/IRX9L*), At5g67230 (*IRX14L*), At3g51610 (*NPU*), and At5g40260 (*RPG1*).

Supplemental data

The following materials are available in the online version of this article.

Supplemental Table S1. Assignment of tetrads from 12 wild-type buds used for immunofluorescence analysis to early, middle, or late substages

Supplemental Table S2. Assignment of tetrads from mutant buds used for immunofluorescence analysis to early, middle, or late substages

Supplemental Figure S1. Additional TEM images of tetrad-stage microspores at the "Golden Gate" stage of PE development.

Supplemental Figure S2. Sections of the 12 wild-type buds stained with Calcofluor White used for the tetrad substage assignment.

Supplemental Figure S3. Distribution of the LM11 xylan epitope in tetrad-containing anthers from all 12 wild-type buds.

Supplemental Figure S4. Distribution of the LM10 xylan epitope in tetrad-containing anthers from all 12 wild-type buds.

Supplemental Figure S5. Distribution of the JIM7 highly-methylesterified pectin epitope in tetrad-containing anthers from all 12 wild-type buds.

Supplemental Figure S6. Distribution of the JIM5 low-methylesterified pectin epitope in tetrad-containing anthers from all 12 wild-type buds.

Supplemental Figure S7. Distribution of the JIM8 arabinogalactan epitope in tetrad-containing anthers from wild-type buds.

Supplemental Figure S8. Distribution of the JIM15 arabinogalactan epitope in tetrad-containing anthers from wild-type buds.

Supplemental Figure S9. Sections of four *spg2 irx14l* buds stained with Calcofluor White used for the tetrad substage assignment.

Supplemental Figure S10. Distribution of the JIM7 highly methylesterified pectin and JIM5 low-methylesterified pectin epitopes in tetrad-containing *spg2 irx14l* double mutant anthers.

Supplemental Figure S11. Sections of four *npu* buds stained with Calcofluor White used for the tetrad substage assignment.

Supplemental Figure S12. Sections of three *rpg1* buds stained with Calcofluor White used for the tetrad substage assignment.

Supplemental Figure S13. Distribution of the LM11 xylan, JIM7 highly-methylesterified pectin, and JIM5 low-methylesterified pectin epitopes in tetrad-containing *rpg1* mutant anthers.

Acknowledgments

We thank Marisa Otegui, Ben August, and Janice Green Pennington (UW-Madison) for their support during our visits to the high-pressure freezer laboratory, Thomas Schuck and Juleen Dickson (UW-Milwaukee) for assisting in anther freezing, and the Dobritsa lab for discussions. We apologize to colleagues whose work we were unable to reference due to space limitations.

Funding

This work was supported by the US National Science Foundation (MCB-1517511 to A.A.D and H.A.O. and MCB-1817835 to A.A.D.), by the Department of Molecular Genetics at OSU (to A.A.D.), and by the Herta Camerer Gross Postdoctoral Research Fellowship (to R.W.).

Conflict of interest statement. The authors declare that they have no competing interests.

References

Aouali N, Laporte P, Clément C (2001) Pectin secretion and distribution in the anther during pollen development in Lilium. Planta **213**: 71–79

Ariizumi T, Hatakeyama K, Hinata K, Inatsugi R, Nishida I, Sato S, Kato T, Tabata S, Toriyama K (2004) Disruption of the novel plant protein NEF1 affects lipid accumulation in the plastids of the tapetum and exine formation of pollen, resulting in male sterility in *Arabidopsis thaliana*. Plant J **39**: 170–181

Ariizumi T, Toriyama K (2011) Genetic regulation of sporopollenin synthesis and pollen exine development. Ann Rev Plant Biol **62**: 437–460

Bidhendi AJ, Chebli Y, Geitmann A (2020) Fluorescence visualization of cellulose and pectin in the primary plant cell wall. J Microsc **278**: 164–181

Blackmore S, Wortley AH, Skvarla JJ, Rowley JR (2007) Pollen wall development in flowering plants. New Phytol **174**: 483–498

Chang HS, Zhang C, Chang YH, Zhu J, Xu XF, Shi ZH, Zhang XL, Xu L, Huang H, Zhang S, et al. (2012) NO PRIMEXINE AND PLASMA MEMBRANE UNDULATION is essential for primexine deposition and plasma membrane undulation during microsporogenesis in Arabidopsis. Plant Physiol **158**: 264–272

Clausen MH, Willats WGT, Knox JP (2003) Synthetic methyl hexagalacturonate hapten inhibitors of anti-homogalacturonan monoclonal antibodies LM7, JIM5 and JIM7. Carbohydrate Res **338**: 1797–1800

Dobritsa AA, Geanconteri A, Shrestha J, Carlson A, Kooyers N, Coerper D, Urbanczyk-Wochniak E, Bench BJ, Sumner LW, Swanson R, et al. (2011) A large-scale genetic screen in Arabidopsis to identify genes involved in pollen exine production. Plant Physiol **157**: 947–970

Fitzgerald MA, Knox RB (1995) Initiation of primexine in freeze-substituted microspores of Brassica campestris. Plant Reprod **8**: 99–104

Gabarayeva NI, Grigorjeva VV (2021) An integral insight into pollen wall development: involvement of physical processes in exine ontogeny in *Calycanthus floridus* L., with an experimental approach. Plant J **105**: 736–753

Guan YF, Huang XY, Zhu J, Gao JF, Zhang HX, Yang ZN (2008) RUPTURED POLLEN GRAIN1, a member of the MtN3/saliva gene family, is crucial for exine pattern formation and cell integrity of microspores in Arabidopsis. Plant Physiol **147**: 852–863

Heslop-Harrison J (1968) Wall development within the microspore tetrad of *Lilium longiflorum*. Can J Bot **46**: 1185–1192

Holdorf MM, Owen HA, Lieber SR, Yuan L, Adams N, Dabney-Smith C, Makaroff CA (2012) Arabidopsis ETHE1 encodes a sulfur dioxygenase that is essential for embryo and endosperm development. Plant Physiol **160**: 226–236

Kang BH (2010) Electron microscopy and high-pressure freezing of Arabidopsis. In T Müller-Reichert, ed, Methods in Cell Biology, Academic Press, Cambridge, MA, pp 259–283

Kiss JZ, Staehelin LA (1995) High pressure freezing. Techniques in Modern Biomedical Microscopy: Rapid Freezing, Freeze Fracture, and Deep Etching. Wiley-Liss, New York, NY, pp 89–104

Li H, Kim YJ, Yang L, Liu Z, Zhang J, Shi H, Huang G, Persson S, Zhang D, Liang W (2020) Grass-specific EPAD1 is essential for pollen exine patterning in rice. Plant Cell **32**: 3961–3977

Li WL, Liu Y, Douglas CJ (2017) Role of glycosyltransferases in pollen wall primexine formation and exine patterning. Plant Physiol **173**: 167–182

Majewska-Sawka A, Rodriguez-Garcia MI (2006) Immunodetection of pectin and arabinogalactan protein epitopes during pollen exine formation of Beta vulgaris L. Protoplasma **228**: 41–47

McCartney L, Marcus SE, Knox JP (2005) Monoclonal antibodies to plant cell wall xylans and arabinoxylans. J Histochem Cytochem **53**: 543–546

Mohnen D (2008) Pectin structure and biosynthesis. Curr Opin Plant Biol **11**: 266–277

Mondol PC, Xu D, Duan L, Shi J, Wang C, Chen X, Chen M, Hu J, Liang W, Zhang D (2020) Defective Pollen Wall 3 (DPW3), a novel alpha integrin-like protein, is required for pollen wall formation in rice. New Phytol **225**: 807–822

Owen HA, Makaroff CA (1995) Ultrastructure of microsporogenesis and microgametogenesis in *Arabidopsis thaliana* (L.) Heynh. ecotype Wassilewskija (Brassicaceae). Protoplasma **185**: 7–21

Pattathil S, Avci U, Baldwin D, Swennes AG, McGill JA, Popper Z, Bootten T, Albert A, Davis RH, Chennareddy C, et al. (2010) A Comprehensive Toolkit of Plant Cell Wall Glycan-Directed Monoclonal Antibodies. Plant Physiol **153**: 514–525

Paxson-Sowders DM, Dodrill CH, Owen HA, Makaroff CA (2001) DEX1, a novel plant protein, is required for exine pattern formation during pollen development in Arabidopsis. Plant Physiol **127**: 1739–1749

Quilichini TD, Douglas CJ, Samuels AL (2014) New views of tapetum ultrastructure and pollen exine development in *Arabidopsis thaliana*. Ann Bot **101**: 501–507

Radja A, Horsley EM, Lavrentovich MO, Sweeney AM (2019) Pollen cell wall patterns form from modulated phases. Cell **176**: 856–868.e10

Rhee SY, Somerville CR (1998) Tetrad pollen formation in *quartet* mutants of *Arabidopsis thaliana* is associated with persistence of pectic polysaccharides of the pollen mother cell wall. Plant J **15**: 79–88

Shi J, Cui M, Yang L, Kim YJ, Zhang D (2015) Genetic and biochemical mechanisms of pollen wall development. Trends Plant Sci **20**: 741–753

Suzuki T, Narciso JO, Zeng W, A van de Meene, Yasutomi M, Takemura S, Lampugnani ER, Doblin MS, Bacic A, Ishiguro S (2017) KNS4/UPEX1: a type II arabinogalactan β-(1,3)-galactosyltransferase required for pollen exine development. Plant Physiol **173**: 183–205

Wang R, Dobritsa AA (2018) Exine and aperture patterns on the pollen surface: Their formation and roles in plant reproduction. Annu Plants Rev Online **1**: 1–40

Wang R, Dobritsa AA (2021) Loss of THIN EXINE2 disrupts multiple processes in the mechanism of pollen exine formation. Plant Physiol **187**: 133–157

Willats WGT, McCartney L, Mackie W, Knox JP (2001) Pectin: cell biology and prospects for functional analysis. Plant Mol Biol **47**: 9–27

Xu D, Mondol PC, Ishiguro S, Shi J, Zhang D, Liang W (2020) NERD1 is required for primexine formation and plasma membrane undulation during microsporogenesis in *Arabidopsis thaliana*. aBIOTECH **1**: 205–218